On the Development of Digital Radiography Detectors : A Review

Ho Kyung Kim[1,#], Ian Alexander Cunningham[2], Zhye Yin[3] and Gyuseong Cho[4]

[1] School of Mechanical Engineering, Pusan National University, Busan 609-735, South Korea
[2] Imaging Research Laboratories, Robarts Research Institute, London, Ontario, Canada N6A 5K8
[3] Computed Tomography System and Application Laboratory, GE Global Research Center, Niskayuna, NY 12309, USA
[4] Department of Nuclear and Quantum Engineering, Korea Advanced Science and Technology, Daejeon 305-701, South Korea
Corresponding Author / E-mail: hokyung@pnu.edu; TEL: +82-51-510-3511; FAX: +82-51-518-4613

KEYWORDS: Digital radiography, Digital X-ray imaging, Flat panel, Scintillator, Photoconductor, Amorphous silicon, Amorphous selenium, Cascaded models

This article reviews the development of flat-panel detectors for digital radiography based on amorphous materials. Important design parameters and developments are described for the two main components of flat-panel detectors: the X-ray converter and the readout pixel array. This article also introduces the advanced development concepts of new detectors. In addition, the cascaded linear systems method is reviewed because it is a very powerful tool for improving the design and assessment of X-ray imaging detector systems.

Manuscript received: August 14, 2008 / Accepted: September 4, 2008

1. Introduction

A broad spectrum of probes, such as high-frequency sound waves, radio-frequency electromagnetic waves, X-rays, and γ-rays, has been used in the medical field to see inside the human body. Of these, X-rays are the most widely used, and projection radiography accounts for the majority of all medical imaging procedures. In spite of a tremendous development effort, however, general radiography has remained an analog technique dominated by screen-film systems. The main reason behind the slow progress is the difficulty and cost to make digital detectors as large as radiographic films, which were introduced more than 100 years ago shortly after Wilhelm Conrad Roentgen discovered the X-ray.[1]

Presently, the most successful commercial detectors for digital radiography (DR) are photostimulable phosphors, also known as storage phosphors, which store the image information created by the absorption of incident X-rays as a latent image. The latent image is a distribution of charges trapped in metastable traps that can be converted into blue-green or ultraviolet light signals by optical stimulation, typically with a red or near-infrared laser beam. Storage phosphor detector technology normally requires human intervention because the storage phosphor cassette must be transferred to a laser scanning station that converts the latent image into a digital image. The first commercial system of this type was introduced by the Fuji Photo Film Co., Ltd., in the early 1980s.[2] Storage phosphor-based imaging systems are referred to as computed radiography (CR) to distinguish them from other digital technologies; the term DR is used to describe digital imaging equipment designed to capture and process images directly without the need for film processing or user intervention. We will not discuss CR systems in this article, but the interested reader can find a comprehensive review article for these systems in the references.[3]

As Yaffe and Rowlands[4] have discussed, numerous alternate technologies have been used in DR systems. Flat-panel detectors (FPDs) based on active-matrix pixel arrays are currently the most successful. The FPD concept was motivated by the flat-panel display industry, which had high ambitions of making large-area active-matrix liquid crystal displays (AMLCDs) in the mid-1980s. While the first FPD prototype was 64 × 40 pixels,[5] an FPD with many millions of pixels 17 × 17 inches in size is now available, matching the size of a standard radiographic film cassette.[6,7]

Two technical schemes are used in digital X-ray imaging with FPDs. The first is the direct conversion scheme[8,9] using photoconductors that permit the conversion of incident X-rays into signal charges, as shown in Fig. 1(a). The second is the indirect conversion scheme[5,10] using scintillators that convert incident X-rays into optical photons, as shown in Fig. 1(b). In signal-readout pixel arrays, the direct conversion scheme uses a two-dimensional (2D) array of pixel electrodes and storage capacitors to collect and read out latent image charges formed on the photoconductor surface. The indirect conversion array uses a 2D photodiode array to collect optical photons emitted from an overlying scintillator and read out the signal charges converted in a photodiode. Both readout pixel arrays incorporate active switching devices, such as diodes or transistors, in each pixel to integrate signal charges in storage capacitors or photodiodes for a period during the off-state of the switching devices, and transfer signal charges to the external readout integrated circuits (ROICs) during the on-state of the switching devices. In other words, an FPD consists mainly of X-ray converters (*i.e.*, scintillators for indirect conversion and photoconductors for direct conversion schemes) and readout pixel arrays. Unlike the direct conversion configuration, optical coupling between the scintillator and the readout pixel array in the indirect conversion scheme is important because, for example, the mismatch of refractive indices between the two components results in a significant loss of optical photons, reducing the X-ray sensitivity.

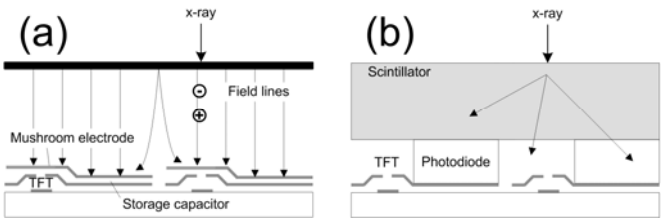

Fig. 1 Schematic of X-ray detection principles with FPDs. (a) Direct-conversion detection. The X-rays absorbed by the photoconductor release *e–h* pairs that drift to the photoconductor surfaces along the applied field lines. There is minimal lateral diffusion of the charge to reduce the spatial resolution. The charges are collected by the pixel electrodes and distributed onto the storage capacitors. The integrated charges are transferred to the external charge integrating amplifiers through the data lines by enabling the pixel thin film transistor (TFT). (b) Indirect conversion detection. The scintillator converts incident X-ray photons into visible light that is absorbed in a thin photodiode layer realized on the readout pixel array, creating *e–h* pairs. The drift motion of these carriers due to the external field applied across the photodiode layer discharges the photodiode, and these integrated charges are transferred to the charge amplifiers through the TFT.

Large-area FPDs are now well-established in the field of medical imaging.[11] Recent medical imaging applications of large-area FPDs include radiography, mammography, fluoroscopy, cardiology, and oncology.[12] This wide spectrum of applications requires a detector with high resolution, wide dynamic range, low noise, fast readout rate, high contrast sensitivity, and scalability. For example, the mammography application requires the highest resolution and the widest dynamic range because of the requirement to image tissue not only very close to the skin but also at the chest wall, and the highest sensitivity because cancerous cells must be distinguished from normal cells. On the other hand, the cardiology application requires a readout rate as fast as 30 fps in continuous operation during an exam. There is, however, no universal detector to cover all the applications mentioned. Instead, a large amount of effort has been invested to develop detectors tailored to each relevant application. As a result of extensive research and development efforts, several medical-equipment companies are now producing digital FPDs to replace film in mammography and radiography applications, and image intensifiers for cardiology and fluoroscopy applications.[7]

Comprehensive reviews of DR detectors are available in many references.[4,13-20] The interested reader can find useful topics not covered in this article in the cited publications and in the references they contain. This article separates the configuration of FPDs into two components: X-ray converters and readout pixel arrays. This article also describes the principles of operation, some important design parameters, and developments of the two components. The development of FPDs is discussed briefly along with a description of new detector development underway. In addition, the cascaded linear systems method, a very powerful tool for the design and assessment of X-ray imaging detector systems, is reviewed.

2. Flat-panel Detectors

2.1 X-ray Converters

DR detector systems can be simply modeled as multiple cascaded image-forming stages.[21,22] These stages could include the detection of individual X-rays and the conversion of these X-rays into secondary quanta (*i.e.*, optical photons in indirect conversion detectors or electrical charges in direct conversion detectors) within an X-ray converter, the escape of secondary quanta from the converter, the collection of the secondary quanta in pixel sensing or storage elements, and the digitization of the stored signals. However, all detectors extract information relating to the X-ray image in the first stage only, *i.e.*, the detection of X-rays. Subsequent stages may result in the loss of information, even if they provide large amplification. This occurs, for example, during the conversion of optical photons in the scintillator, because the information statistically recorded in an image is still limited by the number of X-rays absorbed within the X-ray converter. However, it is still important to maintain a high level of amplification at each stage to prevent the loss of information, although no information can be added to the image.

The *quantum sink*, the stage with the fewest quanta (largest statistical uncertainty), defines the limiting value of the image signal-to-noise ratio (SNR), which is no greater than the square root of the number of quanta at that stage.[21,22] Because information-carrying quanta are lost irrecoverably in the quantum sink, amplification stages following a quantum sink cannot improve the SNR. A well-designed system will have a quantum sink located at the very first image-forming stage, *i.e.*, a *primary* quantum sink, so that the information encoded in the image depends only on the number of X-rays detected by the X-ray converter. Such a system is said to be *X-ray quantum limited*. If the quantum sink corresponds to any other stage, *i.e.*, a *secondary* quantum sink, further losses of information-carrying quanta occur in the imaging system due to the sub-optimal design, and image quality is reduced. For example, lens-coupled detector systems are likely to have a secondary quantum sink at the light collection stage mainly because of the geometrical inefficiency in the luminous flux collected over the solid angle subtended by the lens assembly.[21,23-25] Since X-ray conversion is the first stage in the cascaded imaging chain transferring information to the final user, it is the primary factor that determines the overall performance of a detector system.

2.1.1 Scintillators

The most important requirements in a scintillator used as an X-ray converter in the indirect conversion scheme are the availability of a large area, high light output, and high resolving power. Terbium-doped gadolinium oxysulfide (Gd_2O_2S:Tb) and thallium-doped cesium iodide (CsI:Tl) are the best materials used in practical commercial systems to achieve this.

The Gd_2O_2S:Tb granular phosphor screen is a popular X-ray converter because its technology is well known, and its size, thickness, and flexibility can be handled easily. Furthermore, it is cost-effective. The main variable that determines the performance of commercially available Gd_2O_2S:Tb screens is the coverage or mass thickness. The coverage is the mass of the phosphor coated per unit area (g/cm^2). A typical screen is structured as follows.[26] The screen has a thin overcoat, which is optically diffusive. A phosphor layer of the desired thickness is coated on a polyester support. The support contains TiO_2 to provide a reflectance of about 88% at the 545-nm emission of the phosphor. The purpose of this reflector is to enhance the screen speed. One type of screen has no reflector to maximize the spatial resolution. On the back of the support is an anti-curl layer to keep the screen flat. The phosphor layer is made of Gd_2O_2S:Tb, whose density is 7.3 g/cm^3, the same as the phosphor. The binder is a polyurethane elastomer. Therefore, the effective density of the phosphor layer may be determined by the ratio between the phosphors and organic binders used.

The CsI:Tl scintillator has recently received much attention because of its multiple advantages. First, it can be readily deposited by thermal evaporation at low substrate temperature in the range of 50–250°C,[27] and may be directly evaporated onto a readout pixel array without degrading the properties of active devices in the array. This direct deposition avoids the use of the optical coupling agents, such as optical grease or coupling fluid, between the scintillator and the readout pixel array. Therefore, a FPD could be created at a lower cost without concern for further loss or light spreading through the coupling agents. Second, the CsI:Tl scintillator can be formed in columnar or needle-like structures.[28] This unique structure restricts the sideways diffusion of optical photons, and thus allows high spatial

resolution. Third, the optical photon spectrum emitted by CsI:Tl matches well with the absorption response of hydrogenated amorphous silicon (*a*-Si:H) material,[29] which is usually used to fabricate a photodiode array. Finally, the CsI:Tl scintillator gives the highest light output of any known scintillator.[30]

Van Eijk[31] reviewed articles regarding the development of inorganic scintillators in a wide range of medical-imaging applications. Nikl[32] reviewed phosphors and scintillator materials used specifically for X-ray imaging. Their articles and the references they cite will be very helpful to the reader.

2.1.2 Photoconductors

The performance of an X-ray photoconductor is mainly limited by X-ray sensitivity, noise, and image lag. For higher X-ray sensitivity, a photoconductor should be made of materials with a high atomic number Z because the X-ray interaction probability κ (a linear attenuation coefficient) increases with higher values of Z. More specifically, κ is proportional to Z^n, where n is in the range 4-5.[33] Photoconductors with a higher density and thickness greater than $1/\kappa$ can have a larger X-ray interaction probability, and hence a higher X-ray sensitivity. In addition, a photoconductor should have the lowest possible W-value. The W-value is defined as the average energy required to create a single electron-hole (e–h) pair and is proportional to the bandgap energy E_G. From Klein's empirical relation,[34] W is approximately $2.8E_G$ for semiconductors. For amorphous semiconductors, Que and Rowlands[35] claimed that this should be reduced to about $2.2E_G$.

With respect to the noise property, the photoconductor should have negligible dark current.[36] Dark current has two sources: thermal generation and injection through electrical contacts. Blocking contacts on the photoconductor can limit the dark current due to the thermal generation only. However, the thermal generation current increases as the bandgap narrows. Therefore, there is a tradeoff between the X-ray sensitivity and dark current.

Amorphous materials, which are appropriate for preparation in large areas, suffer from incomplete charge collection and large fluctuations due to the trapping and detrapping of charge carriers by various traps or defects in the bandgap.[37-39] This charge trapping in photoconductors can cause temporal artifacts, such as image lag and ghosting.[40-44] Image lag is the carryover of image charge generated by previous X-ray exposures into subsequent image frames, while ghosting is the change of X-ray sensitivity (*i.e.*, long-term image persistence) as a result of previous exposures.[41,45] The trapped charges may be detrapped and can contribute to the signal in the next readout, producing an image lag. In addition, trapped charges can act as recombination centers for subsequently generated charges, reducing the effective lifetime of mobile charge carriers, and in turn, reducing X-ray sensitivity (ghosting). To avoid or reduce this image lag and ghosting, the photoconductor should have mean drift lengths of the generated charge carriers greater than the thickness of the photoconductor. The mean drift length $\mu\tau F$ is defined as the mean distance traversed by a carrier in an electric field before it is trapped.[13] Here, μ and τ describe the mobility and the lifetime of the charge carrier, respectively, and F is the electric field intensity. In addition to this bulk trapping within a photoconductor layer, image lag and ghosting in a photoconductor-based or direct conversion FPD can arise from other sources, such as charge trapping at the interfaces of the photoconductor layer, charge trapping between pixel electrodes, and incomplete readout of signal charges by electronics.[41,46] Note that amorphous silicon typically used as photodiode materials in indirect conversion detectors has similar problems.[45] However, one study reports that magnitudes of image lag and ghosting are much lower than those of photoconductor-based detectors.[47]

Although the X-ray sensitivity of amorphous selenium (*a*-Se) is no higher than that of the scintillators discussed, *a*-Se has proven to be effective as a photoconductor in the direct conversion scheme with the distinct advantage that it can be readily prepared as a thick film or layer over large areas by straightforward thermal evaporation in a conventional vacuum coater without the need to alter its physical properties.[13] Recently, it has been found that the semiconductors PbI_2 and especially HgI_2 can achieve close to the theoretical X-ray sensitivity, *i.e.*, a W-value of 5 eV, which is nearly a 10-fold improvement.[48] Finding materials appropriate for a direct-detection detector is now an important on-going issue.

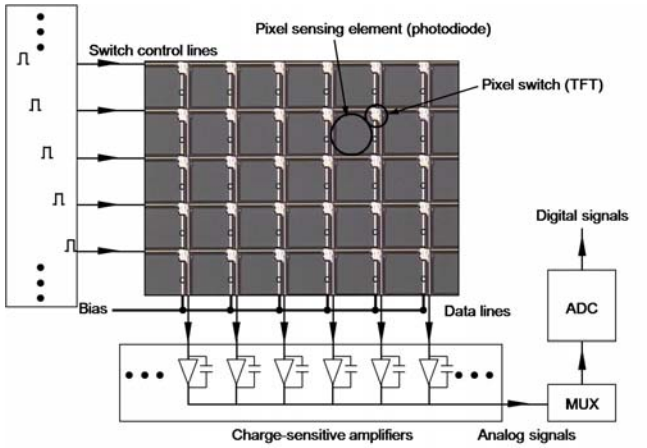

Fig. 2 Schematic of the readout pixel array based on *a*-Si:H photodiode/TFT technology. The reverse-biased photodiode integrates the signal charges during a scanning cycle. The integrated charge signal is transferred and converted to voltage signal through the charge amplifier when the TFT is turned on. The voltage signals are multiplexed column-by-column and converted into digital signals though analog-to-digital converters. The photograph in the figure is courtesy of Samsung Electronics Co. and Vatech Co., Ltd.

2.2 Readout Pixel Arrays

The structure of 2D readout pixel arrays for reading out optical photons emitted from a scintillator, or charge carriers generated in a photoconductor, is similar to a liquid-crystal-skimmed AMLCD, in which each picture element (pixel) is driven by active devices, such as diodes or transistors, arranged in rows and columns to control each pixel. The main structural difference is that the 2D readout pixel array has a photodiode or a storage capacitor near the switching device in each pixel element.

In the direct conversion scheme, the sensing element in each pixel is a simple charge storage capacitor and collection electrode, which can be easily fabricated by dielectric and metal layers. In the indirect conversion scheme, the sensing element is a thin photodiode, in which the absorbed visible light creates e–h pairs. This section presents the readout pixel array for the indirect conversion scheme; the details can be found in the references.[15,16,49] Additional references for readers particularly interested in the design considerations of readout pixel arrays for the direct conversion scheme are also listed.[8,15,50-54]

Figure 2 shows a readout pixel array based on *a*-Si:H photodiode and thin-film transistor (TFT) technology. The photodiode is reverse-biased through a common bias line, and signal charges are accumulated and stored in it during the scanning cycle. When the clock pulse generator of the gate driver sends a gate pulse to each row of the pixel array in sequence, signals from the pixels in the row are read out directly through each data line, and amplified and converted into voltage signals by the array of charge integrating amplifiers. The voltage signals are then multiplexed and converted into digital signals through an analog-to-digital converter (ADC). Figure 3 shows a magnified photograph of a pixel of the *a*-Si:H photodiode/TFT array.

The fabrication of readout pixel arrays is mainly based on the *a*-Si:H process because the *a*-Si:H, which is an alloy of silicon and hydrogen, can be deposited on a large-area glass substrate from the precursor gas state and it exhibits some of the desirable properties of its crystalline counterparts. Amorphous silicon has been known for a

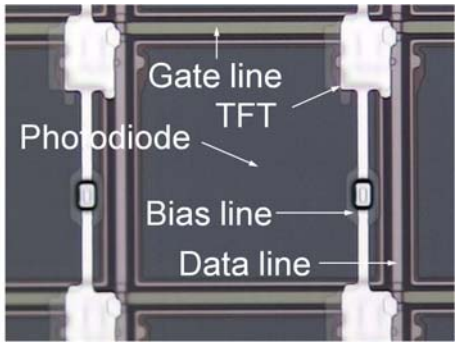

Fig. 3 Microphotograph of the pixel design based on *a*-Si:H photodiode/TFT technology (image courtesy of Samsung Electronics Co. and Vatech Co., Ltd.). The pixel pitch is 143 μm and detailed architectures consisting of the pixel are annotated.

long time, but it only attracted attention as an electronic material once doping to produce *p*-type and *n*-type elements was first demonstrated by Spear and LeComber in 1975.[55] They showed that *p*- and *n*-type semiconductor material could be produced by adding dopant gases, such as diborane (B_2H_6) or phosphine (PH_3), to silane gas (SiH_4). Of the various methods of production from the precursor gas state, plasma-enhanced chemical vapor deposition (PECVD) is known to produce the best quality *a*-Si:H layers.

As a pixel photodiode, the *a*-Si:H *p*-*i*-*n* photodiode is typical because it has high quantum efficiency, low reverse leakage current, and thin-film structure. The configuration consists of an undoped or intrinsic (*i*) layer sandwiched between the top *p*-doped and bottom *n*-doped layers. The *i* layer is relatively thick (about 1 μm) because it interacts mainly with the optical photons emitted from the overlying scintillator. The *n* and *p* layers are very thin and provide rectifying contacts, *i.e.*, ohmic for the majority carriers and blocking for the minority carriers. The optimization of the *p*-layer thickness is very important. It should be thin enough not to attenuate the optical photons significantly, and thick enough to prevent electron injection through the *p*–*i* interface. Metal electrodes should be located on the top and bottom sides to apply a reverse bias on the photodiode. For effective transmission of the scintillation optical photons, a thin metal layer or a transparent conducting layer, such as indium tin oxide (ITO), is used for the top of the photodiode. Conventional AMLCD production lines incorporate only the *n*-doping process because *a*-Si:H TFT does not require the *p*-layer. Modified facilities capable of *p*-doping are required if *a*-Si:H photodiode/TFT arrays are to be fabricated on a conventional AMLCD line. As an alternative, ion-shower doping instead of PECVD has been used to create the *p*-layer.[56] This method can avoid the contamination of the PECVD chambers due to the *p*-doping process. Other approaches to creating *a*-Si:H photodiodes are the use of Schottky barrier diodes[57] and metal-insulator-semiconductor diodes.[58] These designs do not require *p*-doping capability and are more compatible with the process technology required for thin-film *a*-Si:H TFTs, which only require *n*-doping. However, the best quality photodiodes can be obtained using the PECVD method.

Either a diode or TFT can be used as a switching device. The transistor-based readout scheme of the stored charges in a photodiode was originally suggested by Weckler in 1967,[59] and Street *et al.*[5] introduced and successfully demonstrated the *a*-Si:H photodiode/TFT sensor array for digital radiation imaging in 1990. The *a*-Si:H TFT is the inverted staggered type with a gate insulator made from amorphous nitride as a first layer, which is deposited onto a substrate. The next layer is a thin intrinsic *a*-Si:H layer as a main current channel. The other layers are *n*-type *a*-Si:H and metal source and drain contacts, and dielectric and passivation layers. The drain is connected to a pixel photodiode and the source is connected to a common data line followed by the input of the charge integrating amplifier of the external ROIC. The gate contact located below the gate insulator is connected to a common gate line that delivers pulse signals to turn on or off the *a*-Si:H TFT from the external gate drivers. Only *n*-channel *a*-Si:H TFTs are practical because of the low hole mobility.

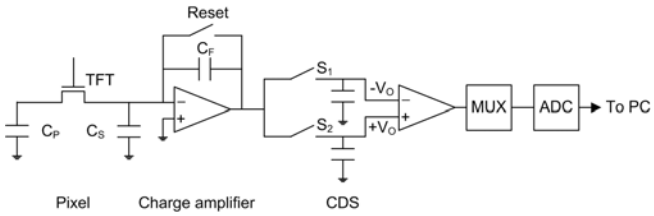

Fig. 4 Schematic of the readout electronics typically used in FPDs. The main components are the charge integrating amplifier, the correlated double sampling circuit, the multiplexer, and the analog-to-digital converter.

When a diode is used as a switching element, a diode switch is connected back-to-back with a pixel photodiode.[60] The diode switch is normally off and the pixel photodiode is reverse-biased during the integration time. Signal charges produced during this time are accumulated on the capacitance of the photodiode. During the readout time, the diode switch is forward-biased by applying a gate pulse, and the charge stored on the photodiode is then discharged. Integration of the discharging current in the charge-integrating amplifier produces an output voltage pulse. The switching diode can be the same type as the pixel photodiode for cost savings in fabrication and high device yield. However, the use of diodes as a switching element has some drawbacks, including highly non-linear characteristics in the forward bias region and hence severe signal variations from pixel to pixel, as well as the interference of signal currents due to a large feed-through transient at the time of the on-off transition. A double-diode switch can be used instead of a single-diode switch. In that case, the feed-through transient charges can be cancelled. Even so, the complex fabrication requirements, such as the large number of interconnections, still remain an important drawback.

As shown in Fig. 4, the readout electronics of a large-area FPD are typically composed of the charge integrating amplifier, correlated double sampling circuit, multiplexer, and the analog-to-digital converter.[50,61-63] The typical principles of operation are as follows. The charge-integrating amplifier is reset before reading the pixel signal, bringing the data line to the amplifier reset potential. This presample voltage $-V_O$ captures the reset noise (*i.e.*, the instantaneous noise sampled on the amplifier feedback capacitor C_F and the parasitic stray capacitance C_S of the readout data line) as well as any offset, and is then stored on the first sample-and-hold capacitor. When the TFT in a pixel is turned on, the signal charge held in the pixel C_P is transferred to C_F. When the charge transfer is completed, a second sample voltage $+V_O$ is stored, and $+V_O$ also contains the reset noise and offset. The difference between two voltage signals is presented to the output through a column multiplexing switch. The reset noise of C_F and C_S, the offset, and any noise whose predominant contribution lies at frequencies less than the reciprocal of the time interval between two sampling processes, are canceled by this correlated double sampling. The output multiplexer delivers signals from all columns onto an output bus before the next row of acquisition can begin. To reduce the demands on the output multiplexer, the sampling and multiplexing operations can be pipelined,[64] so that while the charge from a new row is being integrated, the double samples from the previous row can be multiplexed out.

2.3 Flat-panel Detector Developments

GE HealthCare, a leading medical equipment company, pioneered the development of the indirect conversion FPD with a CsI:Tl scintillator for mammography (1999),[65] radiography (1999),[66] and cardiology (2000).[67] The structure of the GE FPD is shown in Fig. 5. GE HealthCare asserts that the indirect conversion architecture allows independent optimization of the scintillator and photodetection, which

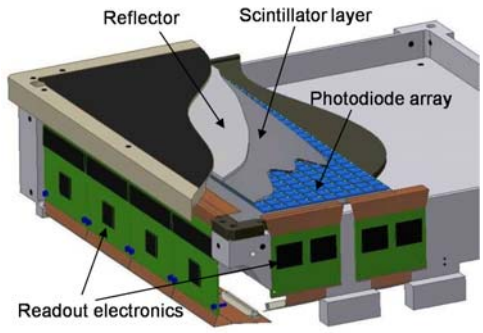

Fig. 5 Cutout diagram of GE FPD (image courtesy of GE Global Research). The peripheral circuits are normally tape-carrier packing-bonded to the panel to reduce the volume of the system and prevent the direct irradiation of X-rays onto the electronics.

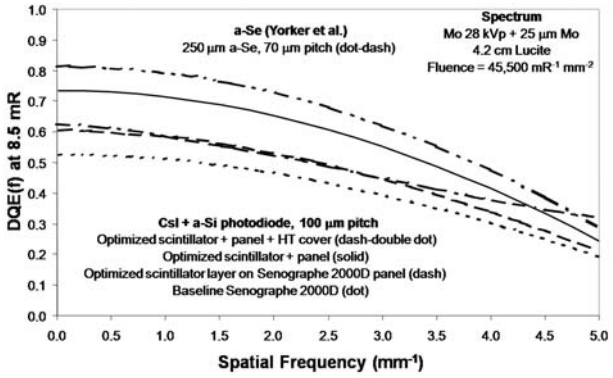

Fig. 6 Detective quantum efficiency (DQE) performance at an exposure of 8.5 mR for the baseline Senographe 2000D detector (dotted) compared to those of a detector with an optimized scintillator layer but the same *a*-Si:H readout pixel array (dashed); a detector with both optimized scintillator and *a*-Si:H readout pixel array (solid); and the projected results for a detector with an optimized scintillator and *a*-Si:H readout pixel array with a high-transmission cover (dash-double dotted). Also shown are the DQE results from the *a*-Se FPD described in the references.[68]

is not possible with *a*-Se technology. Furthermore, they also assert that existing LCD display fabrication technologies can be adapted easily to their type of panel.

The *a*-Se technology developed by Hologic, a leading manufacturer of mammography equipment, is based on the direct conversion mechanism.[68,69] Systems based on the *a*-Se platform sometimes have better imaging characteristics because the thickness of the *a*-Se layer may be increased without sacrificing spatial resolution. Scintillator-based systems should have a scintillator thick enough to stop X-rays and thin enough to reduce the degree of light spreading in that layer, since this affects the spatial resolution. On the other hand, the detection efficiency of a system based on *a*-Se decreases as the *a*-Se layer becomes thicker because the charge carriers may be recombined or absorbed by the *a*-Se layer itself, and thus, the number of charges arriving at the charge-collection electrodes decreases. The *a*-Se-based technology also has cost benefits since the detectors can be manufactured fairly easily by depositing *a*-Se onto commercially available LCD panels, so a full fabrication facility is not required.

Traditionally, spatial resolution is measured using a modulation-transfer function (MTF) that does not consider the signal-to-noise characteristics of a system, but which might dominate the image quality in situations of low or medium contrast. The detective quantum efficiency (DQE) is a more useful metric because it takes both noise and resolution into account to determine if a feature will be

Fig. 7 Photograph showing the *a*-Si:H photodiode/TFT array developed by Samsung Electronics Co. and Vetech Co., Ltd. The panel size is 45 × 46 cm and the active image format is 3072 × 3072 pixels.

detectable.[70,71] The spatial frequency-dependent DQE, DQE(*f*), is dependent on MTF^2(*f*) and reciprocally dependent on the noise power spectrum, NPS(*f*). Figure 6 shows the high-dose DQE performance of the *a*-Si:H-based GE Senographe 2000D detector system used in mammography with various modifications. Also shown is the performance of an *a*-Se-based FPD.[68] Based on the study by Yorker *et al*.,[68] the upper limit to the high-exposure DQE for an *a*-Se-based FPD is estimated to be 70%. An *a*-Si:H-based independent architecture system does not suffer from problems related to charge collection efficiency, and is thus able to deliver a high-dose DQE of more than 80%.[72] At low exposures, an *a*-Se-based platform suffers from its fundamental inefficiency in converting X-rays into detectable signals.[72] More detailed comparisons of commercial mammography systems based on FPD technologies can be found in the references.[73-75] Comparisons of commercial FPDs for DR are also reported in the references.[76-78]

Similar *a*-Si:H-based platforms were also developed independently by other medical equipment companies. In 1997, Siemens Medical Solutions and Philips Medical Systems, two leading medical equipment companies, formed a joint venture company, Trixell, along with Thales Electron Devices. Later, the parent companies of Trixell acquired majority shares in dpiX, securing a consistent supply of amorphous silicon plates. In 2001, Trixell started providing the Pixium 4600 *a*-Si:H-based detector to Siemens and Philips. The focus of dpiX has mainly been the improvement of the *a*-Si:H platform detector by optimizing process and layout.[79,80] On the other hand, Trixell mainly focuses on the adaptation of the *a*-Si:H platform detector to radiography, fluoroscopy,[81] and angiography.[82]

DRTECH Corp. is a Korean company that develops *a*-Se FPDs. The early application of *a*-Se FPDs of 8 × 10 inches in size was for veterinary purposes. Recently DRTECH Corp. has introduced a 17 × 17-inch *a*-Se FPD for general radiography. Another Korean company, Samsung Electronics, has completed the development of *a*-Si:H-based FPD in collaboration with Vatech; it is anticipated that this detector will be available in late 2008. Figure 7 shows the developed *a*-Si:H photodiode/TFT array.

2.4 Advances in Detector Developments

For the performance of DQE(*f*), Moy[83] stated that the ideal MTF should be as large as possible below the Nyquist limit, and then drop rapidly. The ideal MTF could be achieved if the scintillator is structured to match the underlying pixel size of the readout photosensitive elements, as shown in Fig. 8(a). With such a scintillator structure, very little signal at spatial frequencies above the Nyquist frequency and the replication of the spectra would cause little distortion in the signal. A large amount of effort has recently been invested in this new concept of imaging detectors.[84-91] Besides the pixelization of bulk crystalline scintillator by laser dicing, the pixel-structured or pixelated scintillator can be created by several other methods. One is to grow the scintillator on patterned substrates in a pixel-like format.[90] Melting powdered scintillation materials or filling pixel-structured molds with granular phosphors has also been

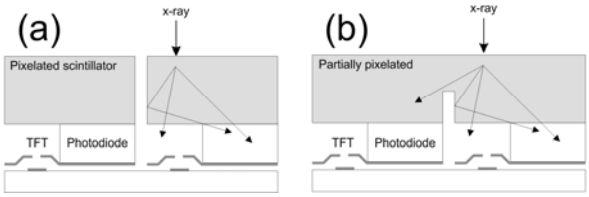

Fig. 8 Design of pixel-structured scintillator-based FPDs. (a) Sketch describing a pixel-structured scintillator in conjunction with the conventional readout pixel array. (b) Conceptual design to reduce the fill factor effect observed in the pixel-structured scintillator design, which reduces the DQE in the low-frequency band.[92]

reported by several groups.[84-89,91] The pixel-structured mold can be realized by deep reactive ion etching or wet etching on silicon wafers,[84,85,87,89,91] or by using a micro-electromechanical system process with silicon wafers or polymer materials, such as SU-8.[86,88] Kim *et al.*[92] reported that the pixelated design is appropriate for high-sensitivity and high-resolution imaging systems, and imagers with a small pixel pitch, such as those employed in mammography or intra-oral imaging, using theoretical and numerical approaches. However, the most significant disadvantage of the pixelated scintillator is the reduction of DQE in the low-frequency band because of the finite fill factor. As a potential means of mitigating this problem, Kim *et al.*[92] proposed the partially pixelated scintillator configuration shown in Fig. 8(b). The concept of the pixel-structured scintillator is attractive to digital X-ray imaging because of the relatively high atomic number and density of the scintillation material, and the possibility of designing a band-limited MTF. Research is active in this area, but many physical hurdles still need to be overcome.

One major issue in the development of DR detectors is low-dose imaging, including dynamic processes such as cardiac imaging and fluoroscopy. Low-dose imaging can be achieved partially by amplifying signals before the signals are delivered to the signal processing electronics. The development of ultra low-noise electronics is another requirement. Such a system would be *X-ray quantum-noise limited*; hence, the noise could not be reduced further and only the random X-ray quantum noise would exist. Antonuk *et al.*[93] described strategies for improving the signal and noise performance of FPDs. One approach is to reduce the additive electronic noise through an improved amplifier, pixel, and array design.[61,63,94,95] An alternative approach is to increase the system gain by various means, including the use of higher gain X-ray converters for direct conversion detectors, such as PbI_2, PbO, HgI_2, and CdZnTe,[96-99] and the use of continuous photodiodes for indirect conversion detectors.[100] Another possible approach to increase the X-ray sensitivity, regardless of the type of detector operation, is to incorporate an amplifier in each pixel.[101-103] Matsuura *et al.*[101] theoretically investigated the signal and noise characteristics of a FPD with amplified pixels by incorporating pixel-level amplifiers, and demonstrated the feasibility of this type of FPD for fluoroscopy. They reported that their design of an amplified pixel detector array could reduce noise more than conventional FPDs, but not low enough to reach the ultimate quantum noise limit for fluoroscopy. This concept has been realized by several groups. Karim *et al.*[102] proposed active pixel architectures based on an amorphous silicon process. Lu *et al.*[103] successfully demonstrated large-area compatible FPDs that contain amplifiers at the pixel level based on excimer laser crystallized poly-Si TFTs. The references[104,105] discuss the potential performance improvements possible using active pixel architectures.

A new concept of indirect conversion FPD with avalanche gain and field emitter array (FEA) readout has recently been proposed for low-dose and high-resolution X-ray imaging.[106-109] It relies on optically coupling a CsI:Tl scintillator to an *a*-Se avalanche photoconductor. The optical photons emitted from the scintillator generate *e–h* pairs near the top of the *a*-Se layer, and they experience avalanche multiplication under high electric field intensity applied within the *a*-Se layer. The amplified charge image is then read out with the electron beams emitted from a 2D FEA, which can be made with pixel sizes down to 50 μm. Therefore, this detector is referred to as a scintillator avalanche photoconductor with high resolution emitter readout (SAPHIRE). The use of the conventional TFT array as a readout device has also been considered by this group.[106,107,110] A similar concept had been proposed much earlier,[109] but the avalanche gain within the *a*-Se layer was not considered.

The technologies for the fabrication of readout pixel arrays have advanced considerably since the introduction of organic semiconductors, and have made impressive improvements in performance for optoelectronic applications.[111] Recently, Street *et al.* developed a novel jet-printing approach or digital lithography for fabricating TFTs, the active matrix arrays for X-ray imaging detectors.[112-116] They have shown that the use of jet-printing techniques in the manufacture of readout pixel arrays provides significant advantages over the conventional processes.[115] First, the production costs could conceivably be reduced. Second, compared to the heavy and fragile glass substrates used in conventional arrays, the printed arrays on plastic substrates would be lighter and more robust. Third, printing techniques could enable the fabrication of significantly larger monolithic arrays than is presently possible for conventional designs. Fourth, flexible arrays would provide an entirely new degree of freedom compared to the existing arrays (*e.g.*, curved and/or conformal imaging detectors).

The DR detectors discussed so far operate in integration mode, *i.e.*, the detectors integrate the incoming signal over the time of the X-ray exposure to acquire an image. Therefore, the resultant image signal is proportional to the deposited energy rather than the number of individual X-ray photons. In this case, we cannot avoid the noise factor due to the distribution of energy deposition in the X-ray converters first identified by Swank,[117] even when the incident X-ray photon is monochromatic. The energy-dependent response of a detector and its related noise can be reduced by operating the detector in the counting mode. Francke *et al.*[118] demonstrated significantly more dose reduction when using the photon-counting method with gaseous avalanche detectors than with screen-film systems. The concept of photon-counting X-ray imaging can provide energy-selective imaging with the adjustment of the upper and lower discriminators, hence windowing the X-ray energies. However, since an individual X-ray photon in high flux needs to be time-resolved and counted with high efficiency in each pixel element of the 2D array for imaging, this photon-counting method requires a highly elaborate detector technology. Llopart *et al.*[119] reported the development of a pixel readout chip, Medipix2, with a pitch of 55 μm in a 256×256-pixel format for reading out charge signals from the overlying X-ray converter. The X-ray converter could be gaseous detectors[119] such as a gas electron multiplier (GEM),[120] Micromegas,[121] or semiconductor detectors[122] such as Si, CdZnTe, or CdTe. Each pixel contains 504 transistors that constitute a charge preamplifier, discriminators, shift registers, digital-to-analog converters, and digital logic. However, problems still remain to be solved for DR applications, such as large-area coverage. Currently available detector configurations are silicon strip detectors,[123] gaseous detectors,[118,124] microchannel plate detectors,[125] and hybrid detectors[122] in which a thick X-ray converter, such as Si,[126] GaAs,[127] CdZnTe,[128] or CdTe,[129] is coupled to customized readout chips (*e.g.*, Medipix series) using a bump-bonding technique. Because of the limitation in detector sizes, photon-counting detectors are currently used for autoradiography,[122,130] mammography,[123,131,132] and computed tomography or tomosynthesis for breast imaging.[125,133] There is a review article available[134] covering the recent developments in the area of semiconductor photon-counting detectors.

3. Cascaded Linear Systems Analysis

Due to the health risks associated with exposure to radiation, and

the risks due to inconclusive or misleading medical diagnoses, technical excellence in medical imaging is critical to high-quality medical care. In radiology, image quality excellence is a balance between system performance and patient radiation dose, and X-ray systems must be designed to ensure the maximum image quality is obtained for the lowest consistent dose. This section describes some of the concepts and methods that are used to quantify, understand, measure, and predict the performance of X-ray detectors and imaging systems.

3.1 The Detective Quantum Efficiency (DQE)

Use of Fourier transform-based metrics to describe spatial resolution in terms of the MTF was introduced to the medical-imaging community by Rossmann *et al.*,[135-137] and is now widely used. The one-dimensional (1D) MTF is defined as the Fourier transform of the line-spread function (LSF):[138]

$$\mathrm{MTF}(u) = \left|\mathcal{F}\{\mathrm{lsf}(x)\}\right| \tag{1}$$

where u is the spatial-frequency variable and lsf(x) is the LSF expressed as a function of position x, normalized to unit area.

Image noise can be described in terms of the auto-covariance function K(x)[139] in the spatial domain, or the image Wiener NPS in the spatial-frequency domain.[138,140,141] The NPS is the spectral decomposition of the noise variance, describing noise in terms of its frequency components:

$$\sigma_d^2 = \int_{-\infty}^{\infty} \mathrm{NPS}_d(u)du \tag{2}$$

where d is the X-ray detector signal and σ_d^2 is the statistical variance in d. The NPS is related to the auto-covariance function by:[139]

$$\mathrm{NPS}(u) = \mathcal{F}\{\mathrm{K}(x)\}. \tag{3}$$

A limitation of the NPS is that its values depend on scaling factors that may be applied by the imaging system and differ from one system to another. This problem was solved by Shaw, who described the image SNR in terms of a noise-equivalent number of quanta (NEQ).[142-144] The NEQ is independent of scaling factors and describes how many Poisson-distributed quanta per unit area would give the same SNR with an ideal imaging system, and thus how many quanta an image is *worth*. This leads directly to what is called the DQE of an imaging system:

$$\mathrm{DQE}(u) \equiv \frac{\mathrm{NEQ}(u)}{\bar{q}_0} = \frac{\bar{q}_0 G^2 \mathrm{MTF}^2(u)}{\mathrm{NPS}_d(u)} \tag{4}$$

$$= \frac{\mathrm{MTF}^2(u)}{\bar{q}_0[\mathrm{NPS}_d(u)/\bar{d}^2]}, \tag{5}$$

where $\bar{q}_0$ is the mean number of X-ray quanta incident per unit area on the detector, $G = \bar{d}/\bar{q}_0$ is the system large-area gain factor, and $\bar{d}$ is the mean detector output value.[145] The MTF and DQE are generally considered to be the most important measures of performance for X-ray imaging systems.

The DQE is sometimes also defined as the transfer of the squared SNR through the imaging system $\mathrm{DQE}(u) = \mathrm{SNR}_{out}^2(u)/\mathrm{SNR}_{in}^2(u)$. However, this is only correct for X-ray imaging where the incident quanta are Poisson distributed (and therefore $\mathrm{SNR}_{in}^2(u) = \bar{q}_0$ [146]), and only when both signal and noise are defined as used in this article. Either Eq. (4) or (5) should be used as the definition of the DQE.

All Fourier methods assume a linear and shift-invariant (LSI) imaging system and wide-sense stationary or wide-sense cyclostationary (WSCS)[145] random noise processes.[139] Linearity means that the detector output value must scale linearly with the input signal. Image pixel values satisfy this requirement only for linear detectors using dark-subtracted *raw* images. Non-linear systems (or systems using non-linear image processing) must be *linearized* before these methods can be used. Shift invariance means that image noise and resolution characteristics are the same at all parts of an image. This assumption may fail near the edges of images.

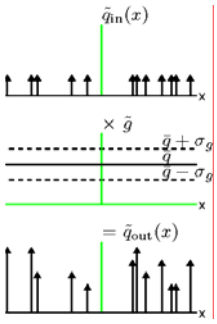

Fig. 9 In a quantum gain process, each input quantum is replaced by $\tilde{g}$ overlapping output quanta where $\tilde{g}$ is an integer random variable with mean $\bar{g}$ and standard deviation σ_g

Equation (5) shows that the DQE of any detector can be determined if the system MTF and the image NPS with the associated mean image pixel value $\bar{d}$ and the incident number of quanta per unit area $\bar{q}_0$ can be determined. Cascaded linear systems theory is powerful because it can be used to determine all these quantities based on system design parameters.

Early linear systems theory used simplistic ideas of noise transfer that ignored the statistical properties of secondary image quanta.[138,147-151] This changed when Rabbani, Shaw, and van Metter described noise transfer through quantum gain and quantum scatter processes.[152,153]

3.2 Elementary Processes in Cascaded Models

Cascaded models of X-ray imaging systems describe how quantum-based images are propagated through a system by cascading simple *elementary* processes. A quantum image is a spatial distribution of quanta, generally in two dimensions. Quanta have negligible size, and a quantum image is represented as a random spatial distribution of Dirac impulse functions $\tilde{q}(\mathrm{r}) = \sum_{i=1}^{N} \delta(\mathrm{r} - \tilde{\mathrm{r}}_i)$,[145,146] where N is the total number of quanta in the image and $\tilde{\mathrm{r}}_i$ is a random vector describing the spatial position of the ith quantum (the overhead $\tilde{}$ is used to indicate a random variable). An imaging system is represented as a series of cascaded processes connecting an input X-ray image $\tilde{q}_0(\mathrm{r})$ to an output image $\tilde{d}(\mathrm{r})$.

3.2.1 Quantum Gain

Quantum gain[145,146,152,154] is a random point process in which each input quantum is replaced by $\tilde{g}$ overlapping output quanta, such as replacing each X-ray quanta with $\tilde{g}$ optical quanta where $\tilde{g}$ is an integer random variable with a mean value $\bar{g}$ and standard deviation σ_g. A graphical representation of this gain process for a 1D distribution is shown in Fig. 9. The output is another quantum image. Values of $\bar{q}$, $\mathrm{T}_{out}(u)$ (the characteristic function), and $\mathrm{NPS}_{out}(u)$ are summarized in Table 1. The output NPS consists of two terms. The first, $\bar{g}^2\mathrm{NPS}_{in}(u)$, describes the transfer of noise by the mean gain $\bar{g}^2$. The second describes additional uncorrelated noise (independent of frequency) resulting from random variations in $\tilde{g}$.

3.2.2 Quantum Selection

Quantum selection with a probability α is a special case of quantum gain, as illustrated in Fig. 10. An example is the quantum efficiency of a radiographic screen.

3.2.3 Quantum Scattering

Quantum scattering is a point process in which each input quantum is randomly relocated to a new position in the image. If the relocation point-spread function is psf(r), the scatter characteristic function is $\mathrm{T}(u) = \mathcal{F}\{\mathrm{psf}(x)\}$. While scattering will normally cause

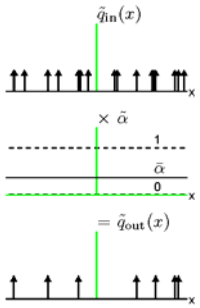

Fig. 10 In a selection process, each input quantum appears in the output with a specified probability

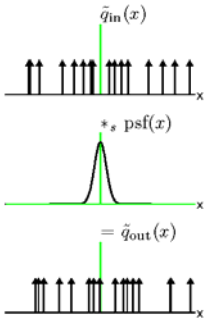

Fig. 11 Each input point is randomly relocated to a new position in the output by the scattering process. The relocation probability density function (PDF) is given by psf(x).

blurring of the output image by T(u), scattering differs from the convolution used to describe the blurring of a linear filter in its noise-transfer properties. The scattering process is illustrated in Fig. 11.

3.2.4 Spatial Integration of Quanta

Digital detectors operate by producing an electrical signal proportional to the number of accumulated image quanta (such as electronic charge) in individual detector elements. This *binning* process is a spatial integration of points that represent interacting quanta. If all quanta incident on an element of width a are detected, the number of quanta interacting in the nth element of a detector element at x is:

$$\tilde{d}_{out}(x) = \int_{x-a_x/2}^{x+a_x/2} \tilde{q}_{in}(x')dx' \tag{6}$$

or simply $\tilde{d}_{out}(x) = \tilde{q}_{in}(x) * \mathbf{II}(x/a_x)$, where $\mathbf{II}(x/a_x)$ is a rectangular function having the value 1 for $-a_x/2 < x < a_x/2$ and 0 elsewhere.

3.2.5 Sampling

Sampling of an analog image to produce a discrete digital image has been presented as an elementary process in cascaded systems by a number of authors[145,155] as multiplication by an infinite train of uniformly-spaced δ functions at intervals of x_0. Thus, in 1D, the output is

$$\tilde{d}^{\dagger}_{out}(x) = \tilde{d}_{in}(x) \times \sum_{n_x=-\infty}^{\infty} \delta(x - n_x x_0) = \sum_{n_x=-\infty}^{\infty} \tilde{d}_n \delta(x - n_x x_0) \tag{7}$$

where the † superscript is used to indicate a discretely sampled function represented as an infinite train of scaled and uniformly spaced δ functions. When $\tilde{d}_{in}(x)$ is a detector presampling signal, the digital image consists of a set of the random values $\tilde{d}_n$.

This sampling process is a linear operation, although it results in a shift-variant output. Fourier-based metrics are still applicable since the output, even in the presence of noise aliasing, is a WSCS random process.

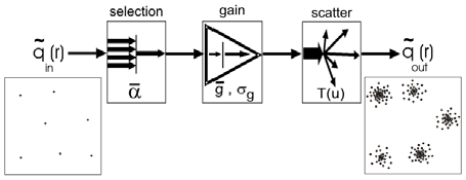

Fig. 12 Simple cascaded model of a radiographic screen consists of quantum selection, gain, and scattering processes

3.3 Simple Systems

Simple systems are modeled by cascading elementary processes where the output of one process becomes a virtual input to the next. Figure 12 shows a cascaded model representing a scintillator as a combination of:

1. quantum selection to select X-rays that interact in the scintillator with probability α;
2. quantum gain representing conversion to light quanta with mean gain $\bar{g}$ and standard deviation σ_g; and
3. quantum scattering representing optical scattering in the scintillator with optical MTF T(u).

The resulting average number of optical quanta per unit area is $\alpha\bar{g}\bar{q}_0$, the MTF is T(u), and the NPS is $\alpha\bar{q}_0(\bar{g}^2 - \bar{g} + \sigma_g^2)\mathrm{T}^2(u) + \alpha\bar{g}\bar{q}_0$. Combining this gives the DQE of the scintillator:

$$\mathrm{DQE}(u) = \frac{\alpha}{1 + \dfrac{\sigma_g^2 - \bar{g}}{\bar{g}^2} + \dfrac{1}{\bar{g}\mathrm{T}^2(u)}}. \tag{8}$$

Several important observations can be made from this simple result:

1. The DQE scales with the quantum efficiency α.

Table 1 Expressions for mean output signal ($\bar{q}_{out}$ for quantum images and $\bar{d}_{out}$ for detector signals), $\mathrm{MTF}_{out}(u)$, and $\mathrm{NPS}_{out}(u)$ for simple processes

Process	Mean Signal	$\mathrm{MTF}_{out}(u)$	$\mathrm{NPS}_{out}(u)$
Quantum Gain, $\bar{g}$, σ_g^2	$\bar{q}_{out} = \bar{g}\bar{q}_{in}$	$\mathrm{MTF}_{in}(u)$	$\bar{g}^2\mathrm{NPS}_{in}(u) + \sigma_g^2\bar{q}_{in}$
Quantum Selection, α	$\bar{q}_{out} = \alpha\bar{q}_{in}$	$\mathrm{MTF}_{in}(u)$	$\alpha^2[\mathrm{NPS}_{in}(u) - \bar{q}_{in}] + \alpha\bar{q}_{in}$
Quantum Scatter, T(u)	$\bar{q}_{out} = \bar{q}_{in}$	$\lvert\mathrm{T}(u)\rvert\mathrm{MTF}_{in}(u)$	$[\mathrm{NPS}_{in}(u) - \bar{q}_{in}]\lvert\mathrm{T}(u)\rvert^2 + \bar{q}_{in}$
Quantum Integration, a	$\bar{d}_{out} = a\bar{q}_{in}$	$\lvert\mathrm{sinc}(au)\rvert\mathrm{MTF}_{in}(u)$	$a^2\mathrm{sinc}^2(au)\mathrm{NPS}_{in}(u)$
Linear Filter, T(u)	$\bar{d}_{out} = \mathrm{T}(0)\bar{d}_{in}$	$\dfrac{\lvert\mathrm{T}(u)\rvert}{\mathrm{T}(0)}\mathrm{MTF}_{in}(u)$	$\lvert\mathrm{T}(u)\rvert^2\mathrm{NPS}_{in}(u)$
Sampling, x_0	$\bar{d}_{out} = \bar{d}_{in}$		$\mathrm{NPS}_{in}(u) + \sum_{n=1}^{\infty}\mathrm{NPS}_{in}\left(u \pm \dfrac{n}{x_0}\right)$

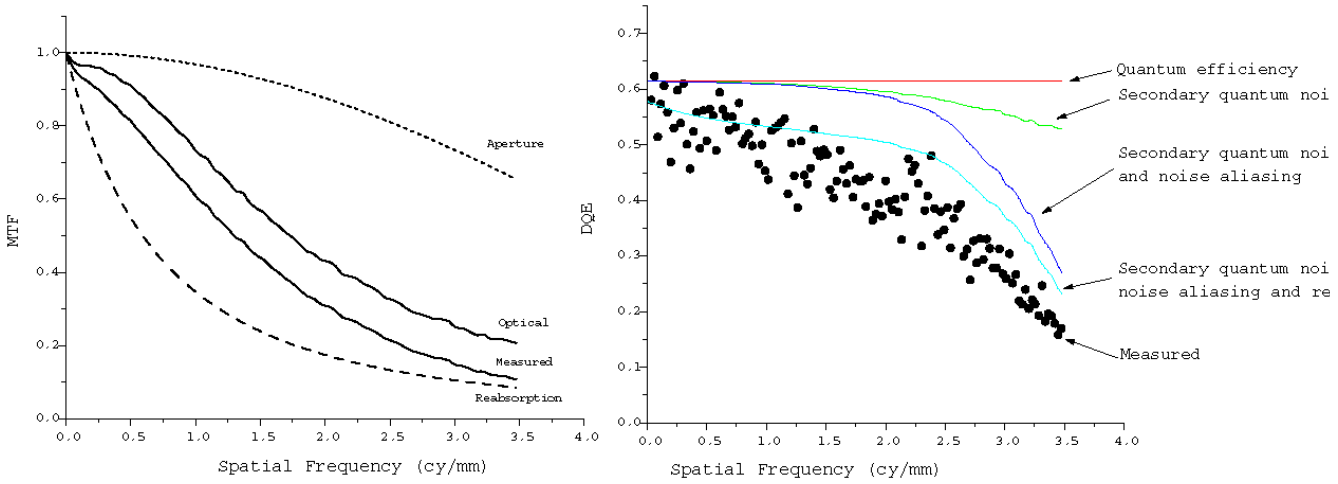

Fig. 13 Left: comparison of measured MTF, theoretical reabsorption MTF $T_K(u)$, estimated optical MTF $T_o(u)$, and aperture (sinc) MTF Right: comparison of measured DQE (117 kV, 4 cm Al) with theoretical model[159]

2. A large optical gain $\bar{g}$ is required to ensure the DQE is close to α. If the optical gain is not sufficiently large, a secondary quantum sink exists that degrades the DQE due to an inadequate number of optical quanta.

3. The optical gain must be particularly large to ensure no secondary quantum sink exists at high spatial frequencies where $T^2(u)$ may be small.

3.4 Complex Systems

The cascaded-systems approach has been used to describe many systems of complex design using different technologies.[92,156-164] Many of these require parallel cascades of simple processes, something that can be achieved with the use of a cross-spectral density term.[154,165] For example, reabsorption of characteristic X-ray emissions in CsI:Tl can be modeled using parallel cascades and can have a substantial effect on image noise and thus the DQE.[158,161] Recent work has extended this approach into the spatiotemporal domain for the description of fluoroscopic systems.[166]

Figure 13 shows both calculated and measured DQE values for an indirect conversion FPD employing CsI:Tl.[159] The cascaded model was used to determine the effect of various processes on the DQE and to make the following observations:

1. A mild secondary quantum sink exists at high spatial frequencies, degrading the DQE by approximately 10% at the sampling cutoff frequency. This loss can be recovered only by increasing the light output from the CsI:Tl, or by improving the light collection efficiency of the FPD.
2. Noise aliasing starts to degrade the DQE at 2.5 cycles/mm and decreases the DQE by approximately 50% at the cutoff frequency. This could be improved by decreasing the detector element size, but this may be impractical.
3. Reabsorption of characteristic X-ray emissions degrades the DQE by approximately 10% over most spatial frequencies. It may not be possible to improve this.

Measured DQE values remain below the cascaded model prediction by up to 15% at frequencies greater than approximately 1 cycle/mm. While the reason for this discrepancy is not yet known, it has recently been shown that X-rays transmitted through the scintillator may interact directly in the readout pixel array and may account for the discrepancy.[26,167]

4. Concluding Remarks

We have briefly reviewed the development of DR detectors in medical imaging. More in-depth knowledge and subjects not covered in this article can be found in the cited publications and the references they contain. Cascaded linear systems theory has been used with great success to describe signal and noise characteristics of many X-ray imaging detectors. It can be used to predict the DQE as well as determine the impact of various physical processes, such as secondary quantum sinks, noise aliasing, reabsorption noise, and others. Additional work will be required to extend this approach to deal with new technological developments and new detector designs. DR detectors are essentially *black boxes* to the end-user. A quick-and-easy way to understand a detector's performance is to check the image quality at the lowest exposure at which a detector is to be used, to identify the intrinsic electronic noise. In addition, the aging property of a detector should be checked by asking the manufacturer, since aging or drift is unavoidable in amorphous semiconductors. The users should also be well versed in calibration procedures, such as offset and gain corrections for the reliable and healthy use of the detector, even though these procedures are normally performed by the manufacturer's software inaccessible to the users. Although large-area FPDs were introduced about three decades ago, the real push to replace film-screen or CR systems is now starting, and companies are up against stiff competition.

ACKNOWLEDGEMENT

H. K. Kim gratefully acknowledges the financial support from the Korea Science and Engineering Foundation through grant R01-2006-000-10233-0 funded by the Korean Ministry of Science and Technology.

REFERENCES

1. Weil, E., “Some Bibliographical Notes on the First Publication on the Roentgen Rays,” Isis, Vol. 29, No. 2, pp. 362-365, 1938.
2. Sonoda, M., Takano, M., Miyahara, J. and Kato, H., “Computed Radiography Utilizing Scanning laser Stimulated Luminescence,” Radiology, Vol. 148, No. 3, pp. 833-838, 1983.
3. Rowlands, J. A., “The Physics of Computed Radiography,” Phys. Med. Biol., Vol. 47, No. 23, pp. R123-R166, 2002.
4. Yaffe, M. J. and Rowlands, J. A., “X-ray Detectors for Digital Radiography,” Phys. Med. Biol. Vol. 42, No. 1, pp. 1-39, 1997.
5. Street, R. A., Nelson, S., Antonuk, L. and Perez-Mendez, V., “Amorphous Silicon Sensor Arrays for Radiation Imaging,” Proc. Mater. Res. Soc., Vol. 192, pp. 441-452, 1990.

6. Floyd, Jr., C. E., Warp, R. J., Dobbins, J. T. III, Chotas, H. G., Baydush, A. H., Vargas-Voracek, R. and Ravin, C. E., "Imaging Characteristics of an Amorphous Silicon Flat-panel Detector for Digital Chest Radiography," Radiology, Vol. 218, No. 3, pp. 683-688, 2001.
7. Kotter, E. and Langer, M., "Digital Radiography with Large-area Flat-panel Detectors," Eur. Radiol., Vol. 12, No. 10, pp. 2562-2570, 2002.
8. Zhao, W. and Rowlands, J. A., "X-ray Imaging Using Amorphous Selenium: Feasibility of a Flat Panel Self-scanned Detector for Digital Radiology," Med. Phys., Vol. 22, No. 10, pp. 1595-1604, 1995.
9. Lee, D. L., Cheung, L. K. and Jeromin, L. S., "A New Digital Detector for Projection Radiography," Proc. SPIE, Vol. 2432, pp. 237-249, 1995.
10. Antonuk, L. E., Boudry, J., Huang, W., McShan, D. L., Morton, E. J., Yorkston, J., Longo, M. J. and Street, R. A., "Demonstration of Megavoltage and Diagnostic X-ray Imaging with Hydrogenated Amorphous Silicon Arrays," Med. Phys., Vol. 19, No. 6, pp. 1455-1466, 1992.
11. James, J. J., Davies, A. G., Cowen, A. R. and O'Connor, P. J., "Developments in Digital Radiography: An Equipment Update," Eur. Radiol., Vol. 11, No. 12, pp. 2616-2626, 2001.
12. Spahn, M., "Flat Detectors and Their Clinical Applications," Eur. Radiol., Vol. 15, No. 9, pp. 1934-1947, 2005.
13. Rowlands, J. and Kasap, S., "Amorphous Semiconductors Usher in Digital X-ray Imaging," Phys. Today, Vol. 50, No. 11, pp. 24-30, 1997.
14. Chotas, H. G., Dobbins, J. T. III and Ravin, C. E., "Principles of Digital Radiography with Large-Area, Electronically Readable Detectors: a Review of the Basics," Radiology, Vol. 210, No. 3, pp. 595-599, 1999.
15. Rowlands, J. A. and Yorkston, J., "Flat Panel Detectors for Digital Radiography," Chapter 4, Handbook of Medical Imaging: Vol. 1. Physics and Psychophysics (Eds. Beutel, J., Kundel, H. L. and Van Metter, R.), SPIE, pp. 223-328, 2000.
16. Street, R. A., "Large Area Image Sensor Arrays," Chapter 4, Technology and Applications of Amorphous Silicon (Ed. R. A. Street), Springer-Verlag, pp. 147-221, 2000.
17. Moy, J.-P., "Recent Developments in X-ray Imaging Detectors," Nucl. Instrum. Meth. A, Vol. 442, No. 1-3, pp. 26-37, 2000.
18. Kasap, S. O. and Rowlands, J. A., "Direct-conversion Flat-panel X-ray Image Detectors," IEE Proc. – Circuits Devices Syst., Vol. 149, No. 2, pp. 85-96, 2002.
19. Antonuk, L. E., El-Mohri, Y., Jee, K.-W., Zhao, Q., Sawant, A., Su, Z. and Street, R. A., "Technological Pathways for 21st Century Active Matrix X-ray Imager Development," Proc. SPIE, Vol. 4682, pp. 1-8, 2002.
20. Yorkston, J., "Recent Developments in Digital Radiography Detectors," Nucl. Instrum. Meth. A, Vol. 580, No. 2, pp. 974-985, 2007.
21. Cunningham, I. A., Westmore, M. S. and Fenster, A., "A Spatial-frequency Dependent Quantum Accounting Diagram and Detective Quantum Efficiency Model of Signal and Noise Propagation in Cascaded Imaging Systems," Med. Phys., Vol. 21, No. 3, pp. 417-427, 1994.
22. Cunningham, I. A. and Shaw, R., "Signal-to-noise Optimization of Medical Imaging Systems," J. Opt. Soc. Am. A, Vol. 16, No. 3, 621-632, 1999.
23. Gagne, R. M., Quinn, P. W., Chen, L., Myers, K. J. and Doyle, R. J., "Optically Coupled Digital Radiography: Sources of Inefficiency," Proc. SPIE, Vol. 4320, pp. 156-162, 2001.
24. Kim, H. K., Cho, G., Lee, S. W., Shin, Y. H. and Cho, H. S., "Development and Evaluation of a Digital Radiographic System Based on CMOS Image Sensor," IEEE Trans. Nucl. Sci., Vol. 48, No. 3, pp. 662-666, 2001.
25. Kim, H. K., Ahn, J. K. and Cho, G., "Development of a Lens-coupled CMOS Detector for X-ray Inspection System," Nucl. Instrum. Meth. A, Vol. 545, No. 1-2, pp. 210-216, 2005.
26. Cho, M. K., Kim, H. K. Graeve, T., Yun, S. M., Lim, C. H., Cho, H. and Kim, J.-M., "Measurements of X-ray Imaging Performance of Granular Phosphors with Direct-coupled CMOS Sensors," IEEE Trans. Nucl. Sci., Vol. 55, No. 3, pp. 1338-1343, 2008.
27. Bates, C. W., "Scintillation Process in Thin Films of CsI(Na) and CsI(Tl) due to Low Energy X-rays, Electrons and Photons," Adv. Electronics Electron Phys., Vol. 28A, pp. 451-459, 1968.
28. Stevels, A. L. N. and Schrama de Pauw, A. D. M., "Vapor-deposited CsI:Na Layers, I. Morphologic and Crystallographic Properties, II. Screen for Application in X-ray Imaging Devices," Philips Res. Rept., Vol. 29, pp. 340-362, 1974.
29. Ito, H., Matsubara, S., Takahashi, T., Shimada, T. and Takeuchi, H., "Integrated Radiation Detectors with *a*-Si Photodiodes on Ceramic Scintillators," Jpn. J. Appl. Phys., Vol. 28, No. 8, pp. L1476-L1479, 1989.
30. Holl, I., Lorenz, E. and Mageras, G., "A Measurement of Light Yield of Some Common Inorganic Scintillators," IEEE Trans. Nucl. Sci., Vol. 35, No. 1, pp. 105-109, 1988.
31. van Eijk, C. W. E., "Inorganic Scintillators in Medical Imaging," Phys. Med. Biol., Vol. 47, No. 8, pp. R85-R106, 2002.
32. Nikl, M., "Scintillation Detectors for X-rays," Meas. Sci. Technol., Vol. 17, No. 4, pp. R37-R54, 2006.
33. Knoll, G. F., "Radiation Detection and Measurement," John Wiley & Sons, p. 49, 2000.
34. Klein, C. A., "Bandgap Dependence and Related Features of Radiation Ionization Energies in Semiconductors," J. Appl. Phys., Vol. 39, No. 4, pp. 2029-2038, 1968.
35. Que, W. and Rowlands, J. A., "X-ray Photogeneration in Amorphous Selenium: Geminate versus Columnar Recombination," Phys. Rev. B, Vol. 51, No. 16, pp. 10500-10507, 1995.
36. Kasap, S. O. and Rowlands, J. A., "Photoconductor Selection for Digital Flat Panel X-ray Image Detectors Based on the Dark Current," J. Vac. Sci. Technol. A, Vol. 18, No. 2, pp. 615-620, 2000.
37. Hack, M., Guha, S. and Shur, M., "Photoconductivity and Recombination in Amorphous Silicon Alloys," Phys. Rev. B, Vol. 30, No. 12, pp. 6991-6999, 1984.
38. Guha, S. and Hack, M., "Dominant Recombination Process in Amorphous Silicon Alloys," J. Appl. Phys., Vol. 58, No. 4, pp. 1683-1685, 1985.
39. Abkowitz, M., "Density of States in *a*-Se from Combined Analysis of Xerographic Potentials and Transient Transport Data," Phil. Mag. Lett., Vol. 58, No. 1, pp. 53-57, 1988.
40. Haugen, C., Kasap, S. O. and Rowlands, J. A., "X-ray Irradiation Induced Bulk Space Charge in Stabilized *a*-Se X-ray Photoconductors," J. Appl. Phys., Vol. 84, No. 10, pp. 5495-5501, 1998.
41. Zhao, W., DeCrescenzo, G. and Rowlands, J. A., "Investigation of Lag and Ghosting in Amorphous Selenium Flat-Panel X-ray Detectors," Proc. SPIE, Vol. 4682, pp. 9-20, 2002.

42. Zhao, B. and Zhao, W., "Temporal Performance of Amorphous Selenium Mammography Detectors," Med. Phys., Vol. 32, No. 1, pp. 128-136, 2005.

43. Zhao, W., DeCresenzo, G., Kasap, S. O. and Rowlands, J. A., "Ghosting Caused by Bulk Charge Trapping in Direct Conversion Flat-panel Detectors Using Amorphous Selenium," Med. Phys., Vol. 32, No. 2, pp. 488-500, 2005.

44. Rau, A. W., Bakueva, L. and Rowlands, J. A., "The X-ray Time of Flight Method for Investigation of Ghosting in Amorphous Selenium-based Flat Panel Medical X-ray Imagers," Med. Phys., Vol. 32, No. 10, pp. 3160-3177, 2005.

45. Siewerdsen, J. H. and Jaffray, D. A., "A Ghost Story: Spatio-temporal Response Characteristics of an Indirect-detection Flat-panel Imager," Med. Phys., Vol. 26, No. 8, pp. 1624-1641, 1999.

46. Kim, H. K., "Analytical Model for Incomplete Signal Generation in Semiconductor Detectors," Appl. Phys. Lett., Vol. 88, Issue 13, pp. 132112-1-132112-3, 2006.

47. Bloomquist, A. K., Yaffe, M. J., Mawdsley, G. E., Hunter, D. M. and Beideck, D. J., "Lag and Ghosting in a Clinical Flat-panel Selenium Digital Mammography System," Med. Phys., Vol. 33, No. 8, pp. 2998-3005, 2006.

48. Street, R. A., Ready, S. E, Melekhov, L., Ho, J., Zuck, A. and Breen, B., "Approaching the Theoretical X-ray Sensitivity with HgI_2 Direct Detection Image Sensors," Proc. SPIE, Vol. 4682, pp. 414-422, 2002.

49. Street, R. A., "Hydrogenated Amorphous Silicon," Cambridge University Press, 1991.

50. Zhao, W., Belvis, I., Germann, S. and Rowlands, J. A., "Digital Radiology Using Active Matrix Readout of Amorphous Selenium: Construction and Evaluation of a Prototype Real-time Detector," Med. Phys., Vol. 24, No. 12, pp. 1834-1843, 1997.

51. Zhao, W., Waechter, D. and Rowlands, J. A., "Digital Radiology Using Active Matrix Readout of Amorphous Selenium: Radiation Hardness of Cadmium Selenide Thin Film Transistors," Med. Phys., Vol. 25, No. 4, pp. 527-538, 1998.

52. Zhao, W., Law, J., Waechter, D., Huang, Z. and Rowlands, J. A., "Digital Radiology Using Active Matrix Readout of Amorphous Selenium: Detectors with High Voltage Protection," Med. Phys., Vol. 25, No. 4, pp. 539-549, 1998.

53. Pang, G., Zhao, W. and Rowlands, J. A., "Digital Radiology Using Active Matrix Readout of Amorphous Selenium: Geometrical and Effective Fill Factors," Med. Phys., Vol. 25, No. 9, pp. 1636-1646, 1998.

54. Zhao, W. and Rowlands, J. A., "Active Matrix X-ray Imaging Array," United States Patent, No. 5,962,856, 1999.

55. Spear W. E. and LeComber P. G., "Substitutional Doping of Amorphous Silicon," Solid State Comm., Vol. 17, No. 9, pp. 1193-1196, 1975.

56. Kim, H. J., Kim, H. K., Cho, G. and Choi, J., "Construction and Characterization of An Amorphous Silicon Flat-panel Detector Based on Ion-shower Doping Process," Nucl. Instrum. Meth. A, Vol. 505, No. 1-2, pp. 155-158, 2003.

57. Munro, P. and Bouius, D. C., "X-ray Quantum Limited Portal Imaging Using Amorphous Silicon Flat-panel Arrays," Med. Phys., Vol. 25, No. 5, pp. 689-702, 1998.

58. Kameshima, T., Kaifu, N., Takami, E., Morishita, M. and Yamazaki, T., "Novel Large Area MIS-type X-ray Image Sensor for Digital Radiography," Proc. SPIE, Vol. 3336, pp. 453-462, 1998.

59. Weckler, G., "Operation of p-n Junction Photodetectors in a Photon Flux Integrating Mode," IEEE J. Solid-Sate Circuit, Vol. 2, No. 3, pp. 65-73, 1967.

60. Graeve, T., Huang, W., Alexander, S. M. and Li, Y., "Amorphous Silicon Image Sensor for X-ray Applications," Proc. SPIE, Vol. 2415, pp. 177-181, 1995.

61. Yarema, R. J., Zimmerman, T., Srage, J., Antonuk, L. E., Berry, J., Huang, W. and Maolinbay, M., "A Programmable, Low Noise, Multichannel ASIC for Readout of Pixelated Amorphous Silicon Arrays," Nucl. Instrum. Meth. A, Vol. 439, No. 2-3, pp. 413-417, 2000.

62. De Geronimo, G., O'Connor, P., Radeka, V. and Yu, B., "Front-end Electronics for Imaging Detectors," Nucl. Instrum. Meth. A, Vol. 471, No. 1-2, pp. 192-199, 2001.

63. Maolinbay, M., Zimmerman, T., Yarema, R. J., Antonuk, L. E., El-Mohri, Y. and Yeakey, M., "Design and Performance of a Low Noise, 128-channel ASIC Preamplifier for Readout of Active Matrix Flat-panel Imaging Arrays," Nucl. Instrum. Meth. A, Vol. 485, No. 1, pp. 661-675, 2002.

64. Huang, W., Antonuk, L. E., Berry, J., Maolinbay, M., Martelli, C., Mody, P., Nassif, S. and Yeakey, M., "An Asynchronous, Pipelined, Electronic Acquisition System for Active Matrix Flat-panel Imagers (AMFPIs)," Nucl. Instrum. Meth. A, Vol. 431, No. 1-2, pp. 273-284, 1999.

65. Vedantham, S., Karellas, A., Suryanarayanan, S., Albagli, D., Han, S., Tkaczyk, E. J., Landberg, C. E., Opsahl-Ong, B., Granfors, P. R., Levis, I., D'Orsi, C. J. and Hendrick, R. E., "Full Breast Digital Mammography with an Amorphous Silicon-based Flat Panel Detector: Physical Characteristics of a Clinical Prototype," Med. Phys., Vol. 27, No. 3, pp. 558-567, 2000.

66. Granfors, P. R. and Aufrichtig, R., "Performance of a 41×41-cm^2 Amorphous Silicon Flat Panel X-ray Detector for Radiographic Imaging Applications," Med. Phys., Vol. 27, No. 6, pp. 1324-1331, 2000.

67. Granfors, P. R., Albagli, D. Tkaczyk, J. E., Aufrichtig, R., Netel, H., Brunst, G., Boudry, J. and Luo, D., "Performance of a Flat Panel Cardiac Detector," Proc. SPIE, Vol. 4320, pp. 77-84, 2001.

68. Yorker, J. G., Jeromin, L. S., Lee, D. L., Palecki, E. F., Golden, K. P. and Zhenxue, J., "Characterization of a Full-field Digital Mammography Detector Based on Direct X-ray Conversion in Selenium," Proc. SPIE, Vol. 4682, pp. 21-29, 2002.

69. Cheung, L. K., Jing, Z., Bogdanovich, S., Golden, K., Robinson, S., Beliaevskaia, E. and Parikh, S., "Image Performance of a New Amorphous Selenium Flat Panel X-ray Detector Designed for Digital Breast Tomosynthesis," Proc. SPIE, Vol. 5745, pp. 1282-1290, 2005.

70. Metz, C. E., Wagner, R. F., Doi, K., Brown, D. G., Nishikawa, R. M. and Myers, K. J., "Toward Consensus on Quantitative Assessment of Medical Imaging Systems," Med. Phys., Vol. 22, No. 7, pp. 1057-1061, 1995.

71. Samei, E., Flynn, M. J., Chotas, H. G. and Dobbins, J. T., "DQE of Direct and Indirect Digital Radiography System," Proc. SPIE, Vol. 4320, pp. 189-197, 2001.

72. Shaw, J., Albagli, D., Wei, C. Y. and Granfors, P. R., "Enhanced *a*-Si/CsI-based Flat panel X-ray Detector for Mammography," Proc. SPIE, Vol. 5368, pp. 370-378, 2004.

73. Rivetti, S., Lanconelli, N., Campanini, R., Bertolini, M., Borasi, G., Nitrosi, A., Danielli, C., Angelini, L. and Maggi, S., "Comparison of Different Commercial FFDM Units by Means of Physical Characterization and Contrast-detail Analysis," Med. Phys., Vol. 33, No. 11, pp. 4198-4209, 2006.

74. Lazzari, B., Belli, G., Gori, G. and Rosselli Del Turco, M., "Physical Characteristics of Five Clinical Systems for Digital Mammography," Med. Phys., Vol. 34, No. 7, pp. 2730-2743,

2007.

75. Monnin, P., Gutierrez, D., Bulling, S., Guntern, D. and Verdun, F. R., "A Comparison of the Performance of Digital Mammography Systems," Med. Phys., Vol. 34, No. 3, pp. 906-914, 2007.
76. Samei, E. and Flynn, M. J., "An Experimental Comparison of Detector Performance for Direct and Indirect Digital Radiography Systems," Med. Phys., Vol. 30, No. 4, pp. 608-622, 2003.
77. Borasi, G., Nitrosi, A., Ferrari, P. and Tassoni, D., "On Site Evaluation of Three Flat Panel Detectors for Digital Radiography," Med. Phys., Vol. 30, No. 7, pp. 1719-1731, 2003.
78. Borasi, G., Samei, E., Bertolini, M., Nitrosi, A. and Tassoni, D., "Contrast-detail Analysis of Three Flat Panel Detectors for Digital Radiography," Med. Phys., Vol. 33, No. 6, pp. 1707-1719, 2006.
79. Weisfield, R. L., Hartney, M., Schneider, R., Aflatooni, K. and Lujan, R., "High Performance Amorphous Silicon Image Sensor for X-ray Diagnostic Medical Imaging Application," Proc. SPIE, Vol. 3659, pp. 307-317, 1999.
80. Weisfield, R. L., Yao, W., Speaker, T., Zhou, K., Colbeth, R. and Proano, C., "Performance Analysis of a 127-micron Pixel Large-area TFT/Photodiode Array with Boosted Fill Factor," Proc. SPIE, Vol. 5368, pp. 338-348, 2004.
81. Ducourant, T., Michel, M. Vieux, G., Peppler, T., Trochet, J. C., Schulz, R. F., Bastiaens, R. J. M. and Busse, F., "Optimization of Key Building Blocks for a Large-area Radiographic and Fluoroscopic Dynamic Digital X-ray Detector Based on *a*-Si:H/CsI:Tl Flat Panel Technology," Proc. SPIE, Vol. 3977, pp. 14-25, 2000.
82. Ducourant, T., Couder, D., Wirth, T., Trochet, J. C., Bastiaens, R. J. M., Bruijins, T. J. C., Luijendijk, H. A., Sandkamp, B., Davies, A. G. and Didier, D., "Image Quality of Digital Subtraction Angiography Using Flat Detector Technology," Proc. SPIE, Vol. 5030, pp. 203-214, 2003.
83. Moy, J.-P., "Signal-to-noise Ratio and Spatial Resolution in X-ray Electronic Imagers: Is the MTF a Relevant Parameter?" Med. Phys., Vol. 27, No. 1, pp. 86-93, 2000.
84. Kleimann, P., Linnros, J., Fröjdh, C. and Petersson, C. S., "An X-ray Imaging Pixel Detector Based on Scintillator Filled Pores in a Silicon Matrix," Nucl. Instrum. Meth. A, Vol. 460, No. 1, pp. 15-19, 2001.
85. Rocha, J. G. and Correia, J. H., "A High-performance Scintillator-silicon-well X-ray Microdetector Based on DRIE Techniques," Sensors and Actuators A, Vol. 92, No. 1-3, pp. 203-207, 2001.
86. Daniel, J. H., Krusor, B., Apte, R. B., Mulato, M., Van Schuylenbergh, K., Lau, R., Do, T., Street, R. A., Goredema, A. and Boils-Boissier, D. C., "Micro-electro-mechanical System Fabrication Technology Applied to Large Area X-ray Image Sensor Arrays," J. Vac. Sci. Technol. A, Vol. 19, No. 4, pp. 1219-1223, 2001.
87. Badel, X., Galeckas, A., Linnros, J., Kleimann, P., Fröjdh, C. and Petersson, C. S., "Improvement of an X-ray Imaging Detector Based on a Scintillating Guides Screen," Nucl. Instrum. Meth. A, Vol. 487, No. 1-2, pp. 129-135, 2002.
88. Tao, S., Gu, Z. H. and Nathan, A., "Fabrication of Gd_2O_2S:Tb Based Phosphor Films Coupled with Photodetectors for X-ray Imaging Applications," J. Vac. Sci. Technol. A, Vol. 20, No. 3, pp. 1091-1094, 2002.
89. Rocha, J. G., Ramos, N. F., Lanceros-Mendez, S., Wolffenbuttel, R.. F. and Correia, J. H., "CMOS X-rays Detector Array Based on Scintillating Light Guides," Sensors and Actuators A, Vol. 110, No. 1-3, pp. 119-123, 2004.
90. Cha, B. K., Bae, J. H., Kim, B.-J., Jeon, H. and Cho, G., "Performance Studies of a Monolithic Scintillator-CMOS Image Sensor for X-ray Application," Nucl. Instrum. Meth. A, Vol. 591, No. 1, pp. 113-116, 2008.
91. Simon, M., Engel, K. J., Menser, B., Badel, X. and Linnros, J., "X-ray Imaging Performance of Scintillator-filled Silicon Pore Arrays," Med. Phys., Vol. 35, No. 3, pp. 968-981, 2008.
92. Kim, H. K., Yun, S. M., Ko, J. S., Cho, G. and Graeve, T., "Cascade Modeling of Pixelated Scintillator Detectors for X-ray Imaging," IEEE Trans. Nucl. Sci., Vol. 55, No. 3, pp. 1357-1366, 2008.
93. Antonuk, L. E., Jee, K.-W., El-Mohri, Y., Maolinbay, M., Nassif, S., Rong, X., Zhao, Q., Siewerdsen, J. H., Street, R. A. and Shah, K. S., "Strategies to Improve the Signal and Noise Performance of Active Matrix, Flat-panel Imagers for Diagnostic X-ray Applications," Med. Phys., Vol. 27, No. 2, pp. 289-306, 2000.
94. El-Mohri, Y., Antonuk, L. E., Zhao, Q., Maolinbay, M., Rong, X., Jee, K.-W., Nassif, S. and Cionca, C., "A Quantitative Investigation of Additive Noise Reduction for Active Matrix Flat-panel Imagers Using Compensation Lines," Med. Phys., Vol. 27, No. 8, pp. 1855-1864, 2000.
95. Beuville, E., Belding, M., Costello, A., Hansen, R. and Petronio, S., "High Performance, Low-noise, 128-channel Readout Integrated Circuit for Flat Panel X-ray Detector Systems," Proc. SPIE, Vol. 5368, pp. 714-725, 2004.
96. Street, R. A., Ready, S. E., Van Schuylenbergh, K., Ho, J., Boyce, J. B. and Nylen, P., "Comparison of PbI_2 and HgI_2 for Direct Detection Active Matrix X-ray Image Sensors," J. Appl. Phys., Vol. 91, No. 5., pp. 3345-3355, 2002.
97. Kasap, S. O., Zahangir Kabir, M. and Rowlands, J. A., "Recent Advances in X-ray Photoconductors for Direct Conversion X-ray Image Detectors," Cur. Appl. Phys., Vol. 6, No. 3, pp. 288-292, 2006.
98. Schieber, M., Zuch, A., Gilboa, H. and Zentai, G., "Reviewing Polycrystalline Mercuric Iodide X-ray Detectors," IEEE Trans. Nucl. Sci., Vol. 53, No. 4, pp. 2385-2391, 2006.
99. Du, H., Antonuk, L. E., El-Mohri, Y., Zhao, Q., Su, Z., Yamamoto, J. and Wang, Y., "Investigation of the Signal Behavior at Diagnostic Energies of Prototype, Direct Detection, Active Matrix, Flat-panel Imagers Incorporating Polycrystalline HgI_2," Phys. Med. Biol., Vol. 53, No. 5, pp. 1325-1351, 2008.
100. Rahn, J. T., Lemmi, F., Weisfield, R. L., Lujan, R., Mei, P. Lu, J.-P., Ho, J., Ready, S. E., Apte, R. B., Nylen, P., Boyce, J. B. and Street, R. A., "High Resolution, High Fill Factor *a*-Si:H Sensor Arrays for Medical Imaging," Proc. SPIE, Vol. 3659, pp. 510-517, 1999.
101. Matsuura, N., Zhao, W., Huang, Z. and Rowlands, J. A., "Digital Radiology Using Active Matrix Readout: Amplified Pixel Detector Array for Fluoroscopy," Med. Phys., Vol. 26, No. 5, pp. 672-681, 1999.
102. Karim, K. S., Nathan, A. and Rowlands, J. A., "Alternative Pixel Architectures for Large Area Medical Imaging," Proc. SPIE, Vol. 4320, pp. 35-46, 2001.
103. Lu, J. P., Van Schuylenbergh, K., Ho, J., Wang, Y., Boyce, J. B. and Street, R. A., "Flat Panel Imagers with Pixel Level Amplifiers Based on Polycrystalline Silicon Thin-film Transistor Technology," Appl. Phys. Lett., Vol. 80, No. 24, pp. 4656-4658, 2002.
104. Antonuk, L. E., Li, Y., Du, H., El-Mohri, Y., Zhao, Q., Yamamoto, J., Sawant, A., Wang, Y., Su, Z., Lu, J.-P., Street, R. A., Weisfield, R. and Yao, B., "Investigation of Strategies to Achieve Optimal DQE Performance from Indirect Detection,

Active Matrix Flat-panel Imagers (AMFPIs) through Novel Pixel Amplification Architectures," Proc. SPIE, Vol. 5745, pp. 18-31, 2005.

105. Antonuk, L. E., El-Mohri, Y., Zhao, Q., Koniczek, M., McDonald, J., Yeakey, M., Wang, Y., Behravan, M., Street, R. A. and Lu, J.-P., "Exploration of the Potential Performance of Polycrystalline Silicon-based Active Matrix Flat-panel Imagers Incorporating Active Pixel Sensor Architectures," Proc. SPIE, Vol. 6913, pp. 69130I-1-69130I-13, 2005.
106. Zhao, W., Hunt, D. C., Tanioka, K. and Rowlands, J. A., "Indirect Flat-panel Detector with Avalanche Gain," Proc. SPIE, Vol. 5368, pp. 150-161, 2004.
107. Zhao, W., Hunt, D. C., Tanioka, K. and Rowlands, J. A., "Amorphous Selenium Flat Panel Detectors for Medical Applications," Nucl. Instrum. Meth. A, Vol. 549, No. 1-3, pp. 205-209, 2005.
108. Zhao, W., Li, D., Rowlands, J. A., Egami, N., Takiguchi, Y., Nanba, M., Honda, Y., Ohkawa, Y., Kubota, M., Tanioka, K., Suzuki, K. and Kawai, T., "An Indirect Flat-panel Detector with Avalanche Gain for Low Dose X-ray Imaging: SAPHIRE (Scintillator Avalanche Photoconductor with High Resolution Emitter Readout)," Proc. SPIE, Vol. 6913, pp. 69130M-1-69130M-11, 2008.
109. Li, D. and Zhao, W., "SAPHIRE (Scintillator Avalanche Photoconductor with High Resolution Emitter Readout) for Low Dose X-ray Imaging: Spatial Resolution," Med. Phys. Vol. 35, No. 7, pp. 3151-3161, 2008.
110. Zhao, W., Li, D., Reznik, A., Lui, B., Hunt, D. C., Tanioka, K. and Rowlands, J. A., "Indirect Flat-panel Detector with Avalanche Gain: Fundamental Feasibility Investigation for SHARP-AMFPI (Scintillator HARP Active Matrix Flat Panel Imager)," Med. Phys. Vol. 32, No. 9, pp. 2954-2966, 2005.
111. Dimitrakopoulos, C. D. and Malenfant, R. L., "Organic Thin Film Transistors for Large Area Electronics," Adv. Mater., Vol. 14, No. 2, pp. 99-117, 2002.
112. Wong, W. S., Ready, S., Matusiak, R., White, S. D., Lu, J.-P., Ho, J. and Street, R. A., "Amorphous Silicon Thin-film Transistors and Arrays Fabricated by Jet Printing," Appl. Phys. Lett., Vol. 80, No. 4, pp. 610-612, 2002.
113. Paul, K. E., Wong, W. S., Ready, S. E. and Street, R. A., "Additive Jet Printing of Polymer Thin-film Transistors," Appl. Phys. Lett., Vol. 83, No. 10, pp. 2070-2072, 2003.
114. Arias, A. C., Ready, S. E., Lujan, R., Wong, W. S., Paul, K. E., Salleo, A., Chabinyc, M. L., Apte, R., Street, R. A., Wu, Y., Liu, P. and Ong, B., "All Jet-Printed Polymer Thin-film Transistor Active-matrix Backplanes," Appl. Phys. Lett., Vol. 85, No. 15, pp. 3304-3306, 2004.
115. Street, R. A., Wong, W. S., Ready, S., Lujan, R., Arias, A. C., Chabinyc, M. L., Salleo, A., Apte, R. and Antonuk, L. E., "Printed Active-Matrix TFT Arrays for X-ray Imaging," Proc. SPIE, Vol. 5745, pp. 7-17, 2005.
116. Ng, T. N., Lujan, R. A., Sambandan, S., Street, R. A., Limb, S. and Wong, W. S., "Low Temperature *a*-Si:H Photodiodes and Flexible Image Sensor Arrays Patterned by Digital Lithography," Appl. Phys. Lett., Vol. 91, No. 6, pp. 063505-1-063505-3, 2007.
117. Swank, R. K., "Absorption and Noise in X-ray Phosphors," J. Appl. Phys., Vol. 44, No. 9, pp. 4199-4203, 1973.
118. Francke, T., Eklund, M., Ericsson, L, Kristoffersson, T., Peskov, V. N., Rantanen, J., Sokolov, S., Soderman, J. E., Ullberg, C. K. and Weber, N., "Dose Reduction Using Photon Counting X-ray Imaging," Proc. SPIE, Vol. 4320, pp. 127-132, 2001.
119. Llopart, X., Campbell, M., Dinapoli, R., San Segundo, D. and Pernigotti, E., "Medipix2: a 64-k Pixel Readout Chip with 55 μm Square Elements Working in Single Photon Counting Mode," IEEE Trans. Nucl. Sci., Vol. 49, No. 5, pp. 2279-2283, 2002.
120. Sauli, F., "GEM: a New Concept for Electron Amplification in Gas Detectors," Nucl. Instrum. Meth. A, Vol. 386, No. 2-3, pp. 531-534, 1997.
121. Giomataris, Y., Rebourgeard, Ph., Robert, J. P. and Charpak, G., "MICROMEGAS: a High-granularity Position-sensitive Gaseous Detectors for High Particle-flux Environments," Nucl. Instrum. Meth. A, Vol. 376, No. 1, pp. 29-35, 1996.
122. Mettivier, G., Montesi, M. C. and Russo, P., "First Images of a Digital Autoradiography System Based on a Medipix2 Hybrid Silicon Pixel Detector," Phys. Med. Biol., Vol. 48, No. 12, pp. N173-N181, 2003.
123. Avila, C., Lopez, J., Sanabria, J. C., Baldazzi, G., Bollini, D., Gombia, M., Cabal, A. E., Ceballos, C., Diz Garcia, A., Gambaccini, M., Taibi, A., Sarnelli, A., Tuffanelli, A., Giubellino, P., Marzari-Chiesa, A., Prino, F., Tomassi, E., Grybos, P., Idzik, M., Swientek, K., Wiacek, P., Montano, L. M., Ramello, L. and Sitta, M., "Contrast Cancellation Technique Applied to Digital X-ray Imaging Using Silicon Strip Detectors," Med. Phys., Vol. 32, No. 12, pp. 3755-3766, 2005.
124. Gobbi, D. G., Dixit, M. S., Dubeau, J. and Johns, P. C., "Photon-counting Radiography with the Gas Microstrip Detector," Phys. Med. Biol., Vol., 44, No. 5, pp. 1317-1335, 1999.
125. Shikhaliev, P. M., Xu, T. and Molloi, S., "Photon Counting Computed Tomography: Concept and Initial Results," Med. Phys., Vol. 32, No. 2, pp. 427-436, 2005.
126. Davidson, D. W., Watt, J., Tlustos, L., Mikulec, B., Campbell, M., Mathieson, K., O'Shea, V., Smith, K. M. and Rahman, M., "Detective Quantum Efficiency of the Medipix Pixel Detector," IEEE Trans. Nucl. Sci., Vol. 50, No. 5, pp. 1659-1663, 2003.
127. Annovazzi, A., Amendolia, S. R., Bigongiari, A., Bisogni, M. G., Catarsi, F., Cesqui, F., Cetronio, A., Colombo, F., Delogu, P., Fantacci, M. E., Gilberti, A., Lanzieri, C., Lavagna, S., Novelli, M., Passuello, G., Paternoster, G., Pieracci, M., Poletti, M., Quattrocchi, M., Rosso, V., Stefanini, A., Testa, A. and Venturelli, L., "A GaAs Pixel Detectors-based Digital Mammographic System: Performances and Imaging Tests Results," Nucl. Instrum. Meth. A, Vol. 576, No. 1, pp. 154-159, 2007.
128. Bertolucci, E., Maiorino, M., Mettivier, G., Montesi, M. C. and Russo, P., "Preliminary Test of an Imaging Probe for Nuclear Medicine Using Hybrid Pixel Detectors," Nucl. Instrum. Meth. A, Vol. 487, No. 1-2, pp. 193-201, 2002.
129. Fröjdh, C., Graafsma, H., Nilsson, H. E. and Ponchut, C., "Characterization of a Pixellated CdTe Detector with Single-photon Processing Readout," Nucl. Instrum. Meth. A, Vol. 563, No. 1, pp. 128-132, 2006.
130. Mettivier, G., Montesi, M. C. and Russo, P., "Digital Autoradiography with a Medipix2 Hybrid Silicon Pixel Detector," IEEE Trans. Nucl. Sci., Vol. 52, No. 1, pp. 46-50, 2005.
131. Thunberg, S., Francke, T., Egerstrom, J., Eklund, M., Ericsson, L., Kristoffersson, T., Peskov, V., Rantanen, J., Sokolov, S., Svedenhag, P., Ullberg, C. K. and Weber, N., "Evaluation of a Photon Counting Mammography System," Proc. SPIE, Vol. 4682, pp. 202-208, 2002.
132. Thunberg, S., Adelow, L., Blom, O., Coster, A., Egerstrom, J.,

Eklund, M., Egnell, P., Francke, T., Jordung, U., Kristoffersson, T., Lindman, K., Lindqvist, L., Marchal, D., Olla, H., Penton, E., Peskov, V., Rantanen, J., Sokolov, S., Svedenhag, P., Ullberg, C. and Weber, N., "Dose Reduction in Mammography with Photon Counting Imaging," Proc. SPIE, Vol. 5368, pp. 457-465, 2004.

133. Maidment, A., Albert, M., Thunberg, S., Adelow, L, Blom, O., Egerstrom, J., Eklund, M., Francke, T., Jordung, U., Kristoffersson, T., Lindman, K., Lindqvist, L, Marchal, D., Olla, H., Penton, E., Rantanen, J., Solokov, S., Ullberg, C. and Weber, N., "Evaluation of a Photon-counting Breast Tomosynthesis Imaging System," Proc. SPIE, Vol. 5745, pp. 572-582, 2005.

134. Mikulec, B., "Development of Segmented Semiconductor Arrays for Quantum Imaging," Nucl. Instrum. Meth. A, Vol. 510, No. 1-2, pp. 1-23, 2003.

135. Rossmann, K., "Measurement of the Modulation Transfer Function of Radiographic Systems Containing Fluorescent Screens," Phys. Med. Biol., Vol. 9, No. 4, pp. 551-557, 1964.

136. Rossmann, K., "The Spatial Frequency Spectrum: a Means for Studying the Quality of Radiographic Imaging Systems," Radiology, Vol. 90, No. 1, pp. 1-13, 1968.

137. Rossmann, K., "Point Spread-function, Line Spread-function, and Modulation Transfer Function. Tools for the Study of Imaging Systems," Radiology, Vol. 93, No. 2, pp. 257-272, 1969.

138. Barrett, H. H. and Swindell, W., "Radiological Imaging – the Theory of Image Foundation, Detection, and Processing," Academic Press, 1981.

139. Papoulis, A., "Probability, Random Variables, and Stochastic Processes," McGraw-Hill, 1991.

140. Jenkins, G. M. and Watts, D. G., "Spectral Analysis and Its Application," Holden-Day Series in Time Series Analysis, Holden-Day, 1968.

141. Giger, M. L., Doi, K. and Metz, C. E., "Investigation of Basic Imaging Properties in Digital Radiography. 2. Noise Wiener Spectrum," Med. Phys., Vol. 11, No. 6, pp. 797-805, 1984.

142. Shaw, R., "The Equivalent Quantum Efficiency of the Photographic Process," J. Photogr. Sc., Vol. 11, pp. 199-204, 1963.

143. Wagner, R. F. and Brown, D. G., "Unified SNR Analysis of Medical Imaging Systems," Phys. Med. Biol., Vol. 30, No. 6, pp. 489-518, 1985.

144. ICRU 54, "Medical Imaging – the Assessment of Image Quality," International Commission of Radiation Units and Measurements, 1995.

145. Cunningham, I. A., "Applied Linear-systems Theory," Chapter 2, Handbook of Medical Imaging: Vol. 1. Physics and Psychophysics (Eds. Beutel, J., Kundel, H. L. and Van Metter, R.), SPIE, pp. 79-159, 2000.

146. Barrett, H. H. and Meyers, K. J., "Foundations of Image Science," Wiley, 2004.

147. Papoulis, A., "Systems and Transforms with Applications in Optics," McGraw-Hill, 1968.

148. Dainty, J. C. and Shaw, R., "Image Science," Academic Press, 1974.

149. Gaskill, J. D., "Linear Systems, Fourier Transforms, and Optics," John Wiley & Sons, 1978.

150. Doi, K., "Field Characteristics of Geometric Unsharpness Due to the X-ray Tube Focal Spot," Med. Phys., Vol. 4, No. 1, pp. 15-20, 1977.

151. Metz, C. E. and Doi, K., "Transfer Function Analysis of Radiographic Imaging Systems," Phys. Med. Biol., Vol. 24, No. 6, pp. 1079-1106, 1979.

152. Rabbani, M. Shaw, R. and van Metter, R. L., "Detective Quantum Efficiency of Imaging Systems with Amplifying and Scattering Mechanisms," J. Opt. Soc. Am. A, Vol. 4, No. 5, pp. 895-901, 1987.

153. Rabbani, M. and van Metter, R. L., "Analysis of Signal and Noise Propagation for Several Imaging Mechanisms," J. Opt. Soc. Am. A, Vol. 6, No. 8, pp. 1156-1164, 1989.

154. Sattarivand, M. and Cunningham, I. A., "Computational Engine for Development of Complex Cascaded Models of Signal and Noise in X-ray Imaging Systems," IEEE Trans. Med. Imag., Vol. 24, No. 2, pp. 211-222, 2005.

155. Zhao, W. and Rowlands, J. A., "Digital Radiology Using Active Matrix Readout of Amorphous Selenium: Theoretical Analysis of Detective Quantum Efficiency," Med. Phys., Vol. 24, No. 12, pp. 1819-1833, 1997.

156. Siewerdsen, J. H., Antonuk, L. E., El-Mohri, Y., Yorkston, J., Huang, W., Boudry, J. M. and Cunningham, I. A., "Empirical and Theoretical Investigation of the Noise Performance of Indirect Detection, Active Matrix Flat-panel Imagers (AMFPIs) for Diagnostic Radiology," Med. Phys., Vol. 24, No. 1, pp. 71-89, 1997.

157. Siewerdsen, J. H., Antonuk, L. E., El-Mohri, Y., Yorkston, J., Huang, W. and Cunningham, I. A., "Signal, Noise Power Spectrum and Detective Quantum Efficiency of Indirect-detection Flat-panel Imagers for Diagnostic Radiology," Med. Phys., Vol. 25, No. 5, pp. 614-628, 1998.

158. Zhao, W., Ji, W. G. and Rowlands, J. A., "Effects of Characteristic X rays on the Noise Power Spectra and Detective Quantum Efficiency of Photoconductive X-ray Detectors," Med. Phys., Vol. 28, No. 10, pp. 2039-2049, 2001.

159. Cunningham, I. A. and Yao, J., "Cascaded Models and the DQE of Flat-panel Imagers: Noise Aliasing, Secondary Quantum Noise and Reabsorption," Proc. SPIE, Vol. 4682, pp. 61-72, 2002

160. Richard, S., Siewerdsen, J. H., Jaffray, D. A., Moseley, D. J. and Bakhtiar, B., "Generalized DQE Analysis of Radiographic and Dual-energy Imaging Using Flat-panel Detectors," Med. Phys., Vol. 32, No. 5, pp. 1397-1413, 2005.

161. Hajdok, G., Yao, J., Battista, J. J. and Cunningham, I. A., "Signal and Noise Transfer Properties of Photoelectric Interactions in Diagnostic X-ray Imaging Detectors," Med. Phys., Vol. 33, No. 10, pp. 3601-3620, 2006.

162. El-Mohri, Y., Antonuk, L. E., Zhao, Q., Wang, Y., Li, Y., Du, H. and Sawant, A., "Performance of a High Fill Factor, Indirect Detection Prototype Flat-panel Imager for Mammography," Med. Phys., Vol. 34, No. 1, pp. 315-327, 2007.

163. Hunt, D. C., Tanioka, K. and Rowlands, J. A., "X-ray Imaging Using Avalanche Multiplication in Amorphous Selenium: Investigation of Depth Dependent Avalanche Noise," Med. Phys., Vol. 34, No. 3, pp. 976-986, 2007.

164. Richard, S. and Siewerdsen, J. H., "Optimization of Dual-energy Imaging Systems Using Generalized NEQ and Imaging Task," Med. Phys., Vol. 34, No. 1, pp. 127-139, 2007.

165. Yao, J. and Cunningham, I. A., "Parallel Cascades: New Ways to Describe Noise Transfer in Medical Imaging Systems," Med. Phys., Vol. 28, No. 10, pp. 2020-2038, 2001.

166. Akbarpour, R., Friedman, S. N., Siewerdsen, J. H., Neary, J. D. and Cunningham, I. A., "Signal and Noise Transfer in Spatiotemporal Quantum-based Imaging Systems," J. Opt. Soc.

Am. A, Vol. 24, No. 12, pp. B151-B164, 2007.

167. Kim, H. K., "Generalized Cascaded Model to Assess Noise Transfer in Scintillator-based X-ray Imaging Detectors," Appl. Phys. Lett., Vol. 89, Issue 23, pp. 233504-1-233504-3, 2006.